Flexible electrical recording from cells using nanowire transistor arrays

Tzahi Cohen-Karni[a], Brian P. Timko[b], Lucien E. Weiss[b], and Charles M. Lieber[a,b,1]

[b]Department of Chemistry and Chemical Biology and [a]School of Engineering and Applied Sciences, Harvard University, Cambridge, MA 02138

Contributed by Charles M. Lieber, March 12, 2009 (sent for review March 5, 2009)

Semiconductor nanowires (NWs) have unique electronic properties and sizes comparable with biological structures involved in cellular communication, thus making them promising nanostructures for establishing active interfaces with biological systems. We report a flexible approach to interface NW field-effect transistors (NWFETs) with cells and demonstrate this for silicon NWFET arrays coupled to embryonic chicken cardiomyocytes. Cardiomyocyte cells were cultured on thin, optically transparent polydimethylsiloxane (PDMS) sheets and then brought into contact with Si-NWFET arrays fabricated on standard substrates. NWFET conductance signals recorded from cardiomyocytes exhibited excellent signal-to-noise ratios with values routinely >5 and signal amplitudes that were tuned by varying device sensitivity through changes in water gate–voltage potential, V_g. Signals recorded from cardiomyocytes for V_g from −0.5 to +0.1 V exhibited amplitude variations from 31 to 7 nS whereas the calibrated voltage remained constant, indicating a robust NWFET/cell interface. In addition, signals recorded as a function of increasing/decreasing displacement of the PDMS/cell support to the device chip showed a reversible >2× increase in signal amplitude (calibrated voltage) from 31 nS (1.0 mV) to 72 nS (2.3 mV). Studies with the displacement close to but below the point of cell disruption yielded calibrated signal amplitudes as large as 10.5 ± 0.2 mV. Last, multiplexed recording of signals from NWFET arrays interfaced to cardiomyocyte monolayers enabled temporal shifts and signal propagation to be determined with good spatial and temporal resolution. Our modular approach simplifies the process of interfacing cardiomyocytes and other cells to high-performance Si-NWFETs, thus increasing the experimental versatility of NWFET arrays and enabling device registration at the subcellular level.

cardiomyocyte | multiplexed recording | nanodevice | PDMS | silicon

Recording electrical signals from cells and tissue is central to areas ranging from the fundamental biophysical studies of function in, for example, the heart and brain, through medical monitoring and intervention (1–3). Over the past several decades, studies of electroactive cells have been carried out by using a variety of recording techniques, including glass micropipette intracellular and patch-clamp electrodes (1, 3), voltage-sensitive dyes (4, 5), multielectrode arrays (MEAs) (6–8), and planar FETs (9–11). The latter 2 recording techniques use well-developed microfabrication methods to allow for direct multiplexed detection on a scale not possible with micropipette technology, although the MEAs and FETs exhibit limited signal-to-noise ratios (S/N) and detection areas that make cellular and subcellular recording difficult (12, 13).

More recently, several groups have demonstrated electrical interfaces with cells and tissue using NWFETs and carbon nanotubes (CNTs) (14–17). Interestingly, studies have shown clearly that NW and CNT devices have substantially higher sensitivity than planar FETs for detection of binding and unbinding of proteins, nucleic acids, and even single virus particles (18–23) and thus can also offer advantages for cellular recording. Indeed, NWFET studies have demonstrated high-S/N recording from cultured neurons, muscle cells and embryonic chicken hearts (14–16). A unique feature of these studies compared with conventional planar devices measurements is that the nanodevices protrude from the plane of substrate, and hence can increase NW/cell interfacial coupling. Indeed, studies have shown that nanostructured interfaces can enhance cellular adhesion and activity (17, 24–28), and thus it is likely that NW and CNT devices have an intrinsic advantage for building interfaces to cells and tissue.

Previous investigations using NW or CNT FETs have not reported multiplexed signal recording from cardiomyocytes, nor has the relationship between interface and signal magnitude been probed. The absence of such results is likely due in part to the difficulty of culturing cells in well-defined orientations over nanoscale devices while maintaining good device characteristics. To address these key issues, we developed a flexible scheme involving cell culture on thin, optically transparent polydimethylsiloxane (PDMS) sheets and subsequent optically registered contact of cells with NWFET arrays.

Results and Discussion

Our NWFET chips were fabricated by using *p*-type silicon NWs as described previously (14, 20, 23, 29). Briefly, aligned Si NWs are assembled on the surface of an oxidized silicon substrate by using shear transfer (30), and then metal source/drain electrodes and interconnects are defined by using photolithography. The metal is passivated with a combination of Si_3N_4 and SU8 dielectric layers. This process yields arrays of addressable Si NWFETs that protrude from the surface of the underlying planar substrate (Fig. 1*A*). Separately, embryonic chicken cardiomyocytes were cultured on 100- to 500-μm-thick, optically transparent rectangular pieces of PDMS (Fig. 1*B*) to form cell monolayers, and then a PDMS/cardiomyocyte substrate was transferred into a well, which contained extracellular medium, over the NWFET chip (Fig. 1*C*). PDMS/cardiomyocyte cell substrates were positioned by using a *x-y-z* manipulator under an optical microscope to bring spontaneously beating cells into direct contact with the NWFETs (Fig. 1*D*). This approach enables us to contact specific monolayer regions with specific devices and subsequently change the region that is being monitored with the NWFETs.

These key features of our experiment can be seen in the photograph of a typical setup (Fig. 2*A*), which highlights the NWFET chip with flexible input/output to recording instruments, PDMS/cell substrate manipulator, and microscope objective. Plots of NWFET conductance (G) vs. applied water-gate voltage (V_g) for 3 representative devices immersed in extracellular medium yield sensitivity values, G/V_g, at $V_g = -0.3$ V of 13.8, 17.2, and 31.1 nS/mV. These sensitivities are similar to our previous studies of NWFET devices fabricated on both rigid and

Author contributions: T.C.-K., B.P.T., and C.M.L. designed research; T.C.-K., B.P.T., and L.E.W. performed research; T.C.-K., B.P.T., and C.M.L. analyzed data; and T.C.-K., B.P.T., L.E.W., and C.M.L. wrote the paper.

The authors declare no conflict of interest.

Freely available online through the PNAS open access option.

[1]To whom correspondence should be addressed. E-mail: cml@cmliris.harvard.edu.

This article contains supporting information online at www.pnas.org/cgi/content/full/0902752106/DCSupplemental.

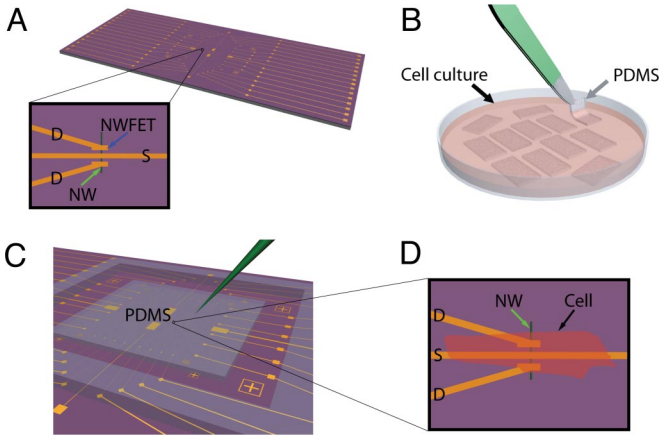

Fig. 1. Schematic of the experimental approach. (*A*) NWFET chip, where NW devices are located at central region of chip. The visible linear features (gold) correspond to NW contacts and interconnect metal. Zoom-in showing a source (S) and 2 drain electrodes (D) connected to a vertically oriented NW (green arrow) defining 2 NWFETs. (*B*) Cardiomyocytes cultured on thin rectangular pieces of PDMS, where the black arrow highlights 1 piece in the culture medium, and the gray arrow indicates 1 piece being removed with tweezers (green). (*C*) PDMS piece with cultured cells oriented over the device region of NWFET chip. The green needle-like structure indicates the probe used to both manipulate the PDMS/cell substrate to specific NW device locations and to apply local force to the NWFET/cell junction. (*D*) Schematic view of a cardiomyocyte (black arrow) oriented over a NW (green arrow) FET device.

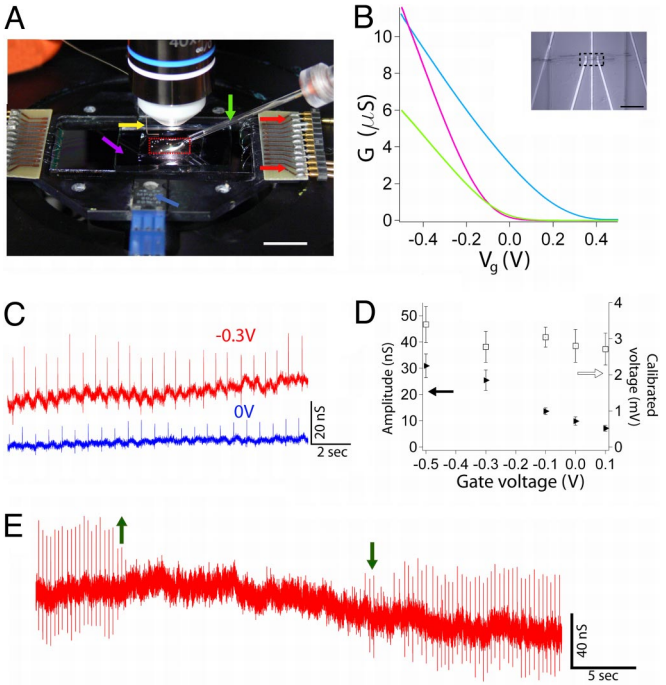

Fig. 2. Measurement of cardiomyocyte signals. (*A*) Photograph of the experimental setup showing the PDMS piece (red dashed box) on top of a NWFET chip within a solution well that is temperature-regulated with an integrated heater (blue arrow). Additional yellow, purple, green, and red arrows highlight positions of the Ag/AgCl reference electrode, solution medium well (length × width × depth = 25–30 × 15–20 × 2 mm^3), glass manipulator/force pipette connected to *x-y-z* manipulator, and plug-in connectors between NWFET interconnect wires and measurement electronics, respectively. (Scale bar, 10 mm.) (*B*) Representative gate responses of 3 Si NWFET devices. The sensitivity (G/V_g) of the separate devices represented by the green, cyan, and purple traces at $V_g = -0.3$ V are 13.8, 17.2, and 31.1 nS/mV, respectively. (*Inset*) Optical microscopy image of a 2 NWFET devices (dashed box) as illustrated schematically in Fig. 1. (Scale bar, 20 μm.) (*C*) Conductance vs. time traces recorded at $V_g = -0.3$ V (red) and 0 V (blue) for the same NWFET–cardiomyocyte interface; the device sensitivities at −0.3 and 0 V were 9.2 and 3.5 nS/mV, respectively. (*D*) Plots of peak conductance amplitude (filled triangles) and calibrated peak voltage amplitude (open squares) vs. V_g; data were obtained from the same experiments shown in *C*. Error bars correspond to ±1 SD. (*E*) Conductance vs. time data recorded as PDMS cardiomyocyte substrate was retracted from the NWFET chip (up arrow) and then brought back into contact with the device chip (down arrow).

flexible plastic substrates (15). In addition, optical images (*Inset*, Fig. 2*B*) show clearly that individual devices can visualize, including S/D electrodes and the NW active element.

Measurement of the conductance versus time from a Si NWFET in contact with a spontaneously beating cardiomyocyte cell monolayer (Fig. 2*C*) yields regularly spaced peaks with a frequency of ≈1.5 Hz and S/N of ≥4. Comparison of the 2 traces (Fig. 2*C*) also shows that the conductance peak magnitude is directly related to the device sensitivity; that is, the data recorded at $V_g = -0.3$ and 0 V had average peak amplitudes of 25.4 ± 3.9 and 9.9 ± 1.6 nS, respectively. Notably, the calibrated voltages for these traces, 2.8 ± 0.4 and 2.8 ± 0.5 mV, were the same within experimental uncertainty. These results confirm the stability of the interface between the NWFETs and PDMS/cardiomyocyte cells and highlight the necessity of recording explicit device sensitivity to interpret corresponding voltages. This important point is further illustrated in the summary of data recorded with V_g values from −0.5 to 0.1 V (Fig. 2*D*), where the conductance signal amplitudes decrease from 31 to 7 nS, respectively, but the calibrated voltage, 2.9 ± 0.3 mV, remained unchanged.

In addition, the signal amplitude can be changed at constant V_g by varying the NWFET–cell interface through manipulation of the PDMS/cardiomyocyte substrate. Conductance versus time data (Fig. 2*E*) demonstrates that the signal from the spontaneously beating cardiomyocyte monolayer gradually vanishes as the PDMS is retracted from the NWFET chip and then emerges again as the PDMS/cells substrate is brought back into contact with the chip. Repeating the retraction/contact sequence yields similar results.

These basic results for NWFET recording from PDMS/cardiomyocyte samples can be compared with previous studies of cardiomyocytes. For example, studies of cardiomyocyte monolayers cultured on conventional planar FET devices have yielded peaks with S/N of 2–6 and amplitudes from 0.2 to 2.5 mV. In general, our NWFETs yield better S/N with values >4 and a maximum of 25 observed (see below). In addition, the typical calibrated voltages recorded in our measurements are similar to or greater than the largest values reported previously. The improvement in peak amplitude is consistent with the fact that the nanodevices protrude from the plane of substrate and hence can increase NW/cell interfacial coupling (17, 24–28) and with our previous studies of cultured neurons (14) and embryonic hearts (15). Recent studies using top-down fabricated NWs also reported millivolt-scale signals, although the cardiomyocytes in this case appeared morphologically undeveloped (e.g., ≈10-μm-diameter spherical structures), and thus it is difficult to compare these results directly with our work and previous planar FET studies.

The ability to manipulate the PDMS/cell substrate independent of the NWFET chip also opens up opportunities compared with cells cultured directly on device arrays. For example, we have carried out experiments to investigate the relationship between recorded signal magnitude and NWFET-PDMS/cell by using a micropipette to displace the PDMS a fixed distance as shown in Fig. 3*A*. Representative conductance versus time data recorded from a spontaneously beating cardiomyocyte monolayer by using the same NWFET device exhibited an increase in

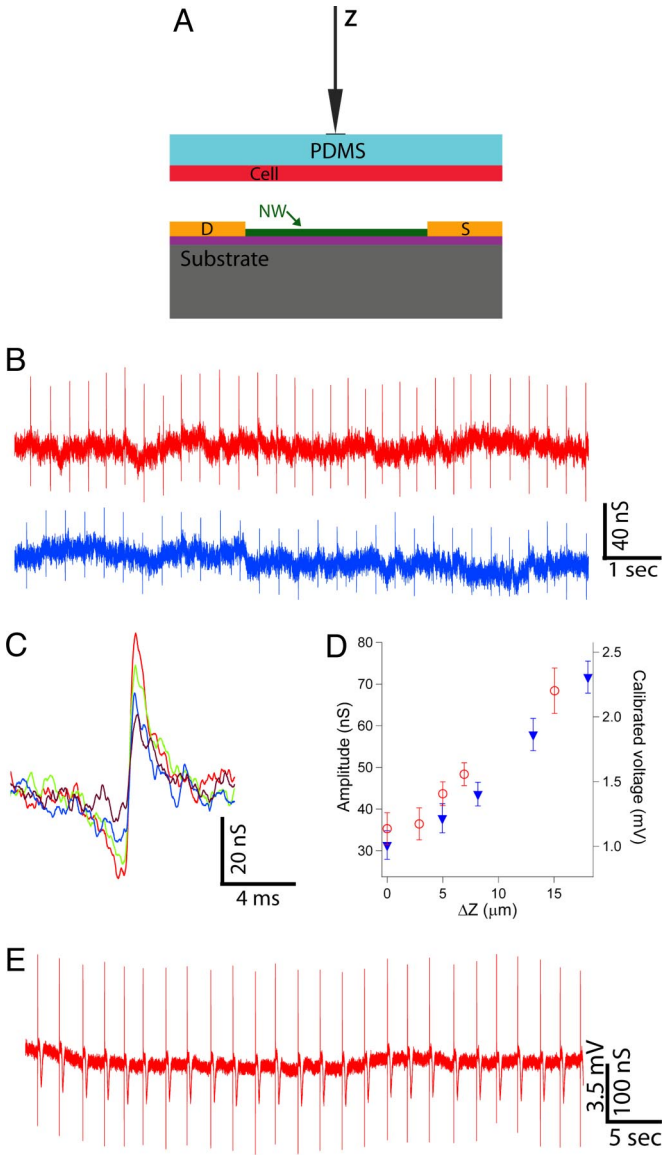

Fig. 3. Effect of applied force on recorded signals. (*A*) Schematic of the experiment illustrating displacement (*Z*) of the PDMS/cell substrate with respect to a NWFET device; displacement is accomplished with micromanipulator-controlled glass pipette. (*B*) Two representative traces recorded with ΔZ values of 8.2 μm (blue) and 18.0 μm (red) yield signal amplitudes of 44 $\pm$ 3 and 72 $\pm$ 4 nS, respectively. The same device was used to record both traces. (*C*) High-resolution comparison of single peaks recorded with ΔZ values of 0 (purple), 8.2 (blue), 13.1 (green), and 18.0 (red) with a corresponding signal increase from 31 to 72 nS. (*D*) Summary of the recorded conductance signals and calibrated voltages vs. ΔZ, where the open red circles (filled blue triangles) were recorded for increasing (decreasing) ΔZ; the small offset (within the error of the measurement) between these 2 directions was due to small lateral displacement during the experiment. (*E*) Data recorded in distinct experiment at large ΔZ close to cell failure with conductance signal amplitude of 299 $\pm$ 7 nS and calibrated voltage of 10.5 $\pm$ 0.2 mV.

peak amplitude from 44 $\pm$ 3 to 72 $\pm$ 4 nS as PDMS was displaced 9.8 μm toward the device. We note in both positions shown that the recorded amplitude was stable, and thus that the changes in NWFET/cell interface are stable. A direct comparison of single peaks recorded for ΔZ values of 0, 8.2, 13.1, and 18.0 μm shows a consistent monotonic increase in peak amplitudes from 31 to 72 nS. In addition, this high-resolution peak comparison demonstrates that there is no observable change in peak shape or

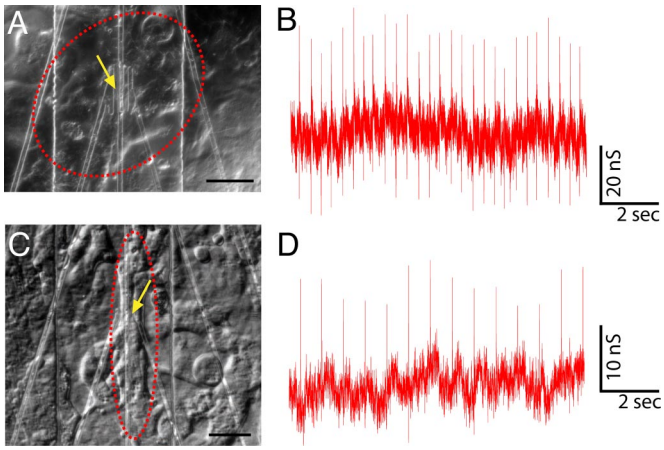

Fig. 4. Recording from distinct regions of cardiomyocyte monolayers. (*A*) A patch of beating cells (red dashed oval) over a NWFET (yellow arrow) with sensitivity of 12.8 nS/mV. (Scale bar, 40 μm.) (*B*) Conductance vs. time signals recorded from the cell patch presented in *A*. The average signal amplitude is 53.2 $\pm$ 4.0 nS. (*C*) Distinct patch of beating cells (red dashed oval) over a NW device (yellow arrow) with sensitivity of 9.2 nS/mV. (Scale bar, 20 μm.) (*D*) Conductance vs. time signals recorded from the cells in *C*. The average signal amplitude is 19.1 $\pm$ 3.1 nS.

peak width over this >2× change in amplitude and that the peak width is consistent with time-scales for ion fluxes associated with ion-channel opening/closing (9).

A plot of our experimental results (Fig. 3*D*) summarizes clearly the systematic 2.3-fold increase in conductance and calibrated voltage peak amplitude and, moreover, demonstrates that these amplitude changes are reversible for experimental data recording on increasing and decreasing PDMS displacement. Last, separate experiments designed to push the limits of PDMS/cell displacement (Fig. 3*E*) showed very large conductance versus time peaks with average conductance amplitude of 299 $\pm$ 7 nS and calibrated voltage of 10.5 $\pm$ 0.2 mV. These results were very stable, suggesting no adverse affect on the cardiomyocytes, although even larger displacements could ultimately lead to irreversible changes and cessation of spontaneous beating. Recent studies of *Aplysia* neurons cultured on planar FET devices have also reported an increase in peak amplitude when the cell body was displaced (31). In both cases, the enhanced signal amplitudes can be attributed to a decrease in gap between the cell membrane and devices, although future studies will be needed to quantify such junction changes.

The ability to manipulate the PDMS/cell substrate independent of the NWFET chip also enables us to identify specific cardiomyocyte regions by using an optical microscope, place the desired cell or cell network over NWFET devices, and then record from the desired region. Two examples are shown in Fig. 4. In the first case, a patch of spontaneously beating cells was located [Fig. 4*A* and supporting information (SI) Movie S1] and placed over a specific device (yellow arrow, Fig. 4*A*). Conductance versus time data was then recorded (Fig. 4*B*) and yielded an average signal amplitude of 53.2 $\pm$ 4.0 nS and relatively large calibrated voltage of 4.2 $\pm$ 0.3 mV. In a second example, a comparatively distinct cell in a cardiomyocyte monolayer was located (red dashed line, Fig. 4*C* and Movie S2) and placed over a different device (yellow arrow, Fig. 4*C*). The recorded conductance versus time data from the spontaneously beating cell yielded an average amplitude of 19.1 $\pm$ 3.1 nS and 2.1 $\pm$ 0.3 mV. Importantly, our ability to identify and register specific cellular regions over NWFET elements has not been demonstrated previously for either planar or nanoscale FET where cells have been cultured directly over device chips. We believe that this

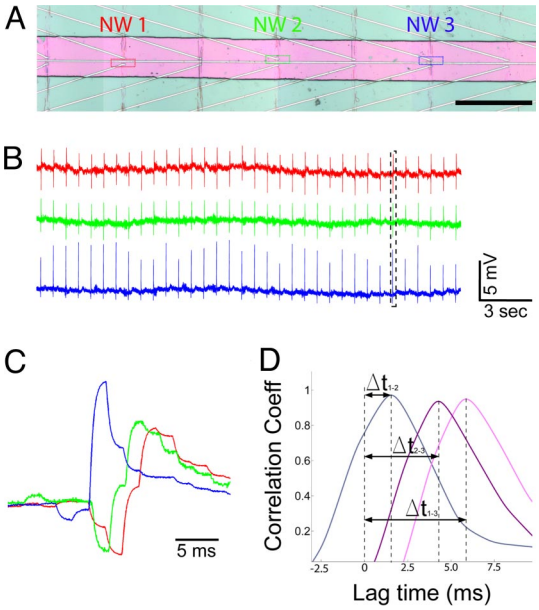

Fig. 5. Multiplexed NWFET recording. (*A*) Optical micrograph showing 3 NWFET devices (NW1, NW2, NW3) in a linear array, where pink indicates the area with exposed NW devices (metal passivated with Si_3N_4) and light green corresponds to the region further passivated with SU8. (Scale bar, 150 μm.) NW1, NW2, and NW3 device sensitivities are 10.9, 10.5, and 17.2 nS/mV, respectively. (*B*) Representative conductance vs. time signals recorded simultaneously from NW1, NW2, and NW3, where the average signals are 50.2 ± 4.6 (4.6 ± 0.4), 42.5 ± 3.2 (4.0 ± 0.3), and 102 ± 15 nS, (5.9 ± 0.9 mV), respectively. (*C*) High-resolution comparison of the temporally correlated peaks highlighted by the black dashed box in *B*. (*D*) Cross-correlation results from recorded signals in *C*. The time shifts Δt_{1-2}, Δt_{2-3}, and Δt_{1-3} correspond to differences between NW1 and 2 (1.5 ms), NW2 and 3 (4.3 ms), and NW1 and 3 (5.9 ms), respectively.

capability will open up a number of interesting studies in the future, including multiplexed recording from well-defined multicellular configurations as well as multiplexed measurements at the single cell level for subcellular resolution investigations.

To this end, we have carried out multiplexed measurements by using the Si NWFET arrays. The devices used in these studies were configured in a linear array (Fig. 5*A*) with an average spacing of 300 μm so that signal propagation within the cardiomyocyte monolayers could be characterized. Simultaneous recording from NW1, NW2, and NW3 devices in contact with spontaneously beating monolayer (Fig. 5*B*) yield very stable and high-S/N (≈10) peaks with amplitudes of 50 ± 5, 43 ± 3, and 102 ± 15 nS, respectively. By using the individually characterized sensitivities for NW1, NW2, and NW3 further gave calibrated voltages of 4.6 ± 0.4, 4.0 ± 0.3, and 5.9 ± 0.9 mV, respectively, where the relatively large magnitude indicates that a good junction is formed between each of the NWFETs and PDMS/cell substrate in the experiment. To determine robustly the time differences between the signals recorded with the 3 devices, we used a cross-correlation methodology (32, 33), although the time difference can also be approximately estimated from comparison single peaks from the 3 devices as shown in Fig. 5*C*. The time shifts between devices derived from the cross-correlation analysis of the full data traces (Fig. 5*D*) show that the average time delay between NW1 and NW2, NW1 and NW3, and NW2 and NW3 is 1.4 ± 0.3, 5.6 ± 0.2, and 4.3 ± 0.3 ms, respectively. These results and device separations yield approximate propagation speeds of 0.07–0.21 m/s that are consistent with measurements on monolayers of neonatal rat cardiomyocytes (4). The variation in propagation speeds is not surprising given the monolayer inhomogeneity and suggests an important future direction. Specifically, we believe that high-resolution multiplexed NWFET recording combined with optical imaging will enable details of both intra- and intercellular propagation to be characterized for well-defined cellular structures.

Conclusions

We have demonstrated a flexible approach to interface silicon NWFETs with cells in which optically transparent PDMS/cell substrates are manipulated to place specific cells over particular NWFET elements. NWFET conductance signals recorded from cardiomyocytes exhibited excellent S/N with values routinely >5 and signal amplitudes that were tuned by varying device sensitivity through changes in V_g. Signals recorded from cardiomyocytes for V_g from −0.5 to +0.1 V exhibited amplitude variations from 31 to 7 nS while the calibrated voltage remained constant, indicating a robust NWFET/cell interface. In addition, signals recorded as a function of increasing the displacement of the PDMS/cell substrate to the NWFET chip showed a reversible 2.3-fold increase in calibrated voltage from 1.0 to 2.3 mV, and independent experiments showed that larger displacement could yield stable signals as large as 10.5 ± 0.2 mV with cell degradation. In addition, multiplexed recording of signals from registered device elements within NWFET arrays interfaced to cardiomyocyte monolayers enabled temporal shifts and signal propagation to be determined with good spatial and temporal resolution. Our modular approach increases the flexibility and opens up opportunities for interfacing cardiomyocytes and other cells to high-performance NWFETs, thus increasing the experimental versatility of NWFET arrays and enabling device registration and studies down to the subcellular level.

Materials and Methods

p-type Si-NWs were synthesized as described previously (14, 20, 23, 29) and were transferred to the surface of oxidized silicon (600-nm-thick oxide; NOVA Electronic Materials, Ltd.) by shear transfer (30). Passivated source and drain electrodes were deposited by using a multilayer photoresist structure (14, 20, 23, 29) consisting of 300-nm LOR3A (Microchem) and 500-nm 1805 (Shipley). After the developing the electrode pattern, the contacts were metallized by thermal evaporation of Ti/Pd/Ti (1/50/10 nm), and then ≈60-nm Si_3N_4 was deposited by plasma-enhanced chemical vapor deposition. Last, the substrate was coated with ≈2- to 15-μm SU-8 photoresist (Microchem), and windows were opened over the NW device regions by photolithography.

Cell culture substrates were made by using Sylgard 184 (Dow Corning, Inc.) polydimethylsiloxane (PDMS) elastomer mixed in a 10:1 ratio of base to curing agent. A known volume of the mixture was cast in a 10 × 10-cm Petri dish to form 100- to 500-μm -hick sheets. The PDMS was cured overnight in an oven at 65 °C, and then cut into ≈4 × 15-mm rectangular pieces. Before cell culture, the PDMS pieces were treated in a UV/ozone cleaner (UV-1; Samco International, Inc) for 8 min at 100 °C, transferred immediately to a 25 μg/mL Fibronectin (BD Biosciences) solution for 1 h, washed twice with phosphate buffer solution, and then air-dried.

White Leghorn chick embryos (Charles River Laboratories) were maintained in a humidified incubator (Carolina Biological Supply Company) at 37.5 °C, and hearts were isolated from embryos at E10–E15 stage. Isolated hearts were immediately transferred to a phosphate buffer solution maintained at 37.5 °C. The hearts were minced and then digested in collagenase II (GIBCO, Inc.) until all of the heart tissue disintegrated into cells. The cell suspension was then centrifuged, and the supernatant was discarded, and the cell pellet was resuspended in 10% FBS DMEM and was incubated for 1 h in a 75-mL flask to clean the cell culture as much as possible from fibroblasts. After 1 h, the cell suspension was collected, cells were counted by using a standard hemocytometer, and were seeded on PDMS thin sections modified with Fibronectin (BD Biosciences Inc) with concentrations varying between 2.5 × 10^5 cells per milliliter to 2 × 10^6 cells per milliliter. The medium was exchanged with N2 (Invitrogen, Inc.) supplemented DMEM:F12 (ATCC, Inc.) medium after 24 h and then every other day. Cells spontaneously contracted after 1–2 days in culture.

All studies were carried at 37.5 °C (except Fig. 4 *C* and *D*, which were carried out at 32 °C) by using Tyrode solution (Sigma–Aldrich Inc.). An Ag/AgCl wire was used as a reference electrode. The NWFET conductance was measured with either AC bias (10 kHz, 30 mV peak-to-peak) or with DC bias set to 150 V by using a battery source. In the case of AC bias, the drain current was

amplified with a variable-gain amplifier (1211 current preamplifier; DL Instruments, Inc.) and filtered by using a lock-in amplifier (DSP dual phase lock-in; Stanford Research Systems) with time constant set to 300 μs; in the case of DC bias, the drain current was amplified with the same variable-gain amplifier. The output data were recorded at an acquisition rate of 40–100 kHz by using a multichannel A/D converter (Digidata 1440A; Molecular Devices) interfaced with a PC running pClamp 10.1 electrophysiology software (Molecular Devices). Postanalysis was completed in Igor Pro (Wavemetrics). ΔZ is defined empirically as the change between Z_i relative to the point the signal can be detected, Z_0; we note that Z_0 is not an absolute point and will depend on the device sensitivity. In addition, to ensure an even pressure distribution, a thin glass rectangle cut from a coverslip (VWR Inc.) was placed on the upper face of the PDMS/cell substrate.

Timing delays were calculated by using a standard cross-correlation technique (32, 33). Briefly, each trace in Fig. 2*B* was loaded in its entirety into Matlab (The Mathworks, Inc.) as a single-column matrix. Each matrix (X_i) was normalized by $X_{i,\mathrm{norm}} = (X_i - \mathrm{mean}(X_i))/\mathrm{std}((X_i - \mathrm{mean}(X_i))$, where mean and std are standard Matlab functions for calculating mean and SD, respectively. Unbiased cross-correlation analysis was performed on pairs of normalized matrices (X_1, X_2) by using the built-in xcorr function. The cross-correlation function ($X_1 * X_2$) is a curve with maximum shifted slightly from zero; this shift represents the time offset between the paired input matrices. The robustness of this technique was tested by examining paired matrices X_1 and X_2, that were either identical or from separate, multiplexed devices that recorded the same signals. We arbitrarily offset X_2 by 400, 20, 10, or 5 points (corresponding to time shifts of 20 ms, 1 ms, 500 μs, and 250 μs, respectively) and observed consistent shifts in the output function $X_1 * X_2$.

ACKNOWLEDGMENTS. We thank K. Kaminitz and R. Milo for helpful discussions. C.M.L acknowledges support of this work by the McKnight Foundation Neuroscience Award and the National Institutes of Health Director's Pioneer Award.

1. Hille B (2001) *Ion Channels of Excitable Membranes* (Sinauer, Sunderland, MA).
2. Zipes DP, Jalife J (2004) *Cardiac Electrophysiology : From Cell to Bedside* (Saunders, Philadelphia).
3. Dhein S, Mohr FW, Delmar M (2005) *Practical Methods in Cardiovascular Research* (Springer, Berlin).
4. Fast VG, Kleber AG (1994) Aniosotropic conduction in monolayers of neonatal rat-heart cells cultured on collagen. *Circ Res* 75:591–595.
5. Kleber AG, Rudy Y (2004) Basic mechanisms of cardiac impulse propagation and associated arrhythmias. *Physiol Rev* 84:431–488.
6. Halbach MD, Egert U, Hescheler J, Banach K (2003) Estimation of action potential changes from field potential recordings in multicellular mouse cardiac myocytes cultures. *Cell Physiol Biochem* 13:271–284.
7. Heer F, et al. (2007) Single-chip microelectronic system to interface with living cells. *Biosens Bioelectron* 22:2546–2553.
8. Meyer T, Boven KH, Gunther E, Fejtl M (2004) Micro-electrode arrays in cardiac safety pharmacology: A novel tool to study QT interval prolongation. *Drug Safety* 27:763–772.
9. Ingebrandt S, Yeung CK, Krause M, Offenhausser A (2001) Cardiomyocytes-transistor-hybrids for sensor application. *Biosens Bioelectron* 16:565–570.
10. Ingebrandt S, Yeung CK, Staab W, Zetterer T, Offenhausser A (2003) Backside contacted field effect transistor array for extracellular signal recording. *Biosens Bioelectron* 18:429–435.
11. Yeung CK, Ingebrandt S, Krause M, Offenhausser A, Knoll W (2001) Validation of the use of field effect transistors for extracellular signal recording in pharmacological bioassays. *J Pharmacol Toxicol Methods* 45:207–214.
12. Prohaska OJ, Olcaytug F, Pfundner P, Dragaun H (1986) Thin-film multiple electrode probes: Possibilities and limitations. *IEEE Trans Biomed Eng* 33:223–229.
13. Banks DJ, Balachandran W, Richards PR, Ewins D (2002) Instrumentation to evaluate neural signal recording properties of micromachined microelectrodes inserted in invertebrate nerve. *Physiol Meas* 23:437–448.
14. Patolsky F, et al. (2006) Detection, stimulation and inhibition of neuronal signals with high-density nanowires transistor arrays. *Science* 313:1100–1104.
15. Timko BP, et al. (2009) Electrical recording from hearts with flexible nanowire device arrays. *Nano Lett* 9:914–918.
16. Pui TS, Agarwal A, Ye F, Balasubramanian N, Chen P (2009) CMOS-compatible nanowire sensor arrays for detection of cellular bioelectricity. *Small* 5:208–212.
17. Cellot G, et al. (2009) Carbon nanotubes might improve neuronal performance by favoring electrical shortcuts. *Nat Nanotech* 4:126–133.
18. Gruner G (2006) Carbon nanotubes trasistors for biosensing applications. *Anal Bioanal Chem* 384:322–335.
19. Patolsky F, Timko BP, Zheng GF, Lieber CM (2007) Nanowire-based nanoelectronic devices in the life sciences. *MRS Bull* 32:142–149.
20. Zheng G, Patolsky F, Cui Y, Wang WU, Lieber CM (2005) Multiplexed electrical detection of cancer markers with nanowires sensor array. *Nat Biotechnol* 23:1294–1301.
21. Stern E, et al. (2007) Label-free immunodetection with CMOS-compatible semiconductiong nanowires. *Nature* 445:519–522.
22. Star A, et al. (2006) Label-free detection of DNA hybridization using carbon nanotubes network field-effect transistors. *Proc Natl Acad Sci USA* 103:921–926.
23. Patolsky F, et al. (2004) Electrical detection of single viruses. *Proc Natl Acad Sci USA* 101:14017–14022.
24. Sniadecki N, Desai RA, Ruiz SA, Chen CS (2006) Nanotechnology for cell–substrate interactions. *Ann Biomed Eng* 34:59–74.
25. Stevens MM, George JH (2005) Engineering the cell surface interface. *Science* 310:1135–1138.
26. Arnold M, et al. (2004) Activation of integrin function by nanopatterned adhesive interfaces. *Chem Phys Chem* 5:383–388.
27. Gheith MK, Sinani VA, Wicksted JP, Matts RL, Kotov NA (2005) Single-walled carbon nanotubes polyelectrolyte multilayers and freestanding films as a biocompatible platform for neuroprosthetic implants. *Adv Mater* 17:2663–2670.
28. Park J, Bauer S, von der Mark K, Schmuki P (2007) Nanosize and vitality:TiO_2 nanotube directs cell fate. *Nano Lett* 7:1686–1691.
29. Patolsky F, Zheng G, Lieber CM (2006) Fabricaton of silicon nanowire devices for ultrasensitive, label-free, real-time detection of biological and chemical species. *Nat Protocols* 1:1711–1724.
30. Javey A, Nam S, Friedman RS, Yan H, Lieber CM (2007) Layer-by-layer assembly of nanowires for three-dimensional, multifunctional electronics. *Nano Lett* 7:773–777.
31. Cohen A, Shappir J, Yitzchaik S, Spira ME (2008) Reversible transition of extracellular field potential recordings of action potentials generated by neurons grown on transistors. *Biosens Bioelectron* 23:811–819.
32. Augustijn CH, Arts T, Prinzen FW, Reneman RS (1991) Mapping the sequence of contraction of the canine left-ventricle. *Pflug Arch Eur J Phys* 419:529–533.
33. Dayan P, Abbott LF (2001) *Theoretical Neuroscience :Computational and Mathematical Modeling of Neural Systems*, eds Sejnowski TJ, Poggio T (MIT Press, Cambridge, MA), pp 27–29.